Cell Reports

4-Hydroxybenzoic acid rescues multisystemic disease and perinatal lethality in a mouse model of mitochondrial disease

Graphical abstract

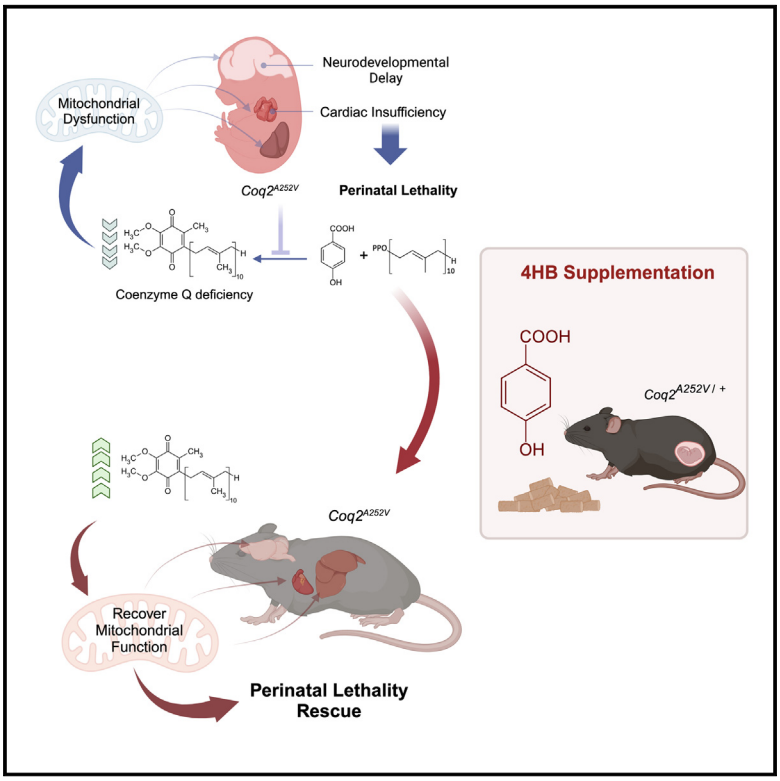

Highlights

- A *Coq2* pathogenic variant induces cardiac insufficiency and neurodevelopmental delay in mice
- Consequently, mice with *Coq2* mutations exhibit perinatal lethality
- 4HB stimulates mitochondrial metabolism in human cells and mice with *COQ2* defects
- 4HB rescues multisystemic disease and prevents perinatal lethality in the $Coq2^{A252V}$ model

Authors

Julia Corral-Sarasa,
Juan Manuel Martínez-Gálvez,
Pilar González-García, ...,
Catarina M. Quinzii,
María Elena Díaz-Casado, Luis C. López

Correspondence

luisca@ugr.es

In brief

Corral-Sarasa et al. highlight the therapeutic efficacy of 4HB in primary coenzyme Q deficiency caused by pathogenic variants in *COQ2*, as demonstrated in human cells and a mouse model. This compound rescues multisystemic disease and perinatal lethality, suggesting potential translational applications of 4HB therapy.

Corral-Sarasa et al., 2024, Cell Reports *43*, 114148
May 28, 2024
https://doi.org/10.1016/j.celrep.2024.114148

Cell Reports

CellPress
OPEN ACCESS

Report

4-Hydroxybenzoic acid rescues multisystemic disease and perinatal lethality in a mouse model of mitochondrial disease

Julia Corral-Sarasa,[1,2,8] Juan Manuel Martínez-Gálvez,[2,3,8] Pilar González-García,[1,2,4] Olivia Wendling,[5] Laura Jiménez-Sánchez,[1] Sergio López-Herrador,[1,2,4] Catarina M. Quinzii,[6] María Elena Díaz-Casado,[1,2,4] and Luis C. López[1,2,4,7,9,*]

[1]Instituto de Investigación Biosanitaria ibs.Granada, 18016 Granada, Spain
[2]Departamento de Fisiología, Facultad de Medicina, Universidad de Granada, 18016 Granada, Spain
[3]Biofisika Institute (CSIC, UBV-EHU) and Department of Biochemistry and Molecular Biology, University of Basque Country, 48940 Leioa, Spain
[4]Instituto de Biotecnología, Centro de Investigación Biomédica, Universidad de Granada, 18016 Granada, Spain
[5]Université de Strasbourg, CNRS, INSERM, CELPHEDIA, PHENOMIN, Institut Clinique de la Souris (ICS), 1 rue Laurent Fries, 67404 Illkirch, France
[6]Department of Neurology, Columbia University Medical Center, New York, NY 10032, USA
[7]Centro de Investigación Biomédica en Red Fragilidad y Envejecimiento Saludable (CIBERFES), 18016 Granada, Spain
[8]These authors contributed equally
[9]Lead contact
*Correspondence: luisca@ugr.es
https://doi.org/10.1016/j.celrep.2024.114148

SUMMARY

Coenzyme Q (CoQ) deficiency syndrome is conventionally treated with limited efficacy using exogenous CoQ_{10}. Poor outcomes result from low absorption and bioavailability of CoQ_{10} and the clinical heterogenicity of the disease. Here, we demonstrate that supplementation with 4-hydroxybenzoic acid (4HB), the precursor of the benzoquinone ring in the CoQ biosynthetic pathway, completely rescues multisystemic disease and perinatal lethality in a mouse model of CoQ deficiency. 4HB stimulates endogenous CoQ biosynthesis in tissues of *Coq2* mutant mice, normalizing mitochondrial function and rescuing cardiac insufficiency, edema, and neurodevelopmental delay. In contrast, exogenous CoQ_{10} supplementation falls short in fully restoring the phenotype. The treatment is translatable to human use, as proven by *in vitro* studies in skin fibroblasts from patients with pathogenic variants in *COQ2*. The therapeutic approach extends to other disorders characterized by deficiencies in the production of 4HB and early steps of CoQ biosynthesis and instances of secondary CoQ deficiency.

INTRODUCTION

Coenzyme Q (CoQ) is an endogenous lipophilic molecule that plays a crucial role in various metabolic pathways through the Q-junction. It is essential for energy metabolism and the regulation of the cell's redox state.[1] In mammals, CoQ biosynthesis is a complex process divided into three compartmentalized phases (Figure S1): (1) cytosolic biosynthesis of 4-hydroxybenzoic acid (4HB), derived from tyrosine through both 4-hydroxyphenylpyruvate dioxygenase-like protein (HPDL)-dependent and HPDL-independent pathways,[2,3] (2) polyprenoid tail biosynthesis, which involves the mevalonate pathway (cytosolic) and polyprenyl diphosphate synthase (PDSS1/PDSS2) activity (mitochondrial),[2] and (3) mitochondrial condensation of the 4HB and the polyprenoid tail, a reaction catalyzed by COQ2, and the subsequent modifications of the quinone ring catalyzed by various enzymes of complex Q.[2,4] Under physiological conditions, the cellular and tissue levels of CoQ are seemingly regulated by the concentration and availability of 4HB and/or the quantity of COQ2.[5]

Pathogenic variants in genes encoding proteins involved in CoQ biosynthesis lead to primary CoQ deficiency, a mitochondrial syndrome with heterogeneous clinical presentations.[6] Among those, pathogenic variants in early steps of the CoQ biosynthetic pathway (e.g., *HPDL*, *PDSS1*, *PDSS2*, or *COQ2*) result in neurodevelopmental disorders, encephalopathy, seizures, sensorineural hearing loss, nephrotic syndrome, cardiomyopathy, and/or edema.[6,7] However, the underlying mechanisms of this clinical heterogeneity remain poorly understood.

The standard treatment for CoQ deficiencies includes oral supplementation with high doses of CoQ_{10}. However, less than 30% of patients with primary CoQ deficiency treated with exogenous CoQ_{10} show significant clinical improvement.[8] In patients with neurological symptoms,[8] this response is particularly inadequate due to CoQ limited absorption and bioavailability, hindering its ability to reach cellular mitochondria.[9]

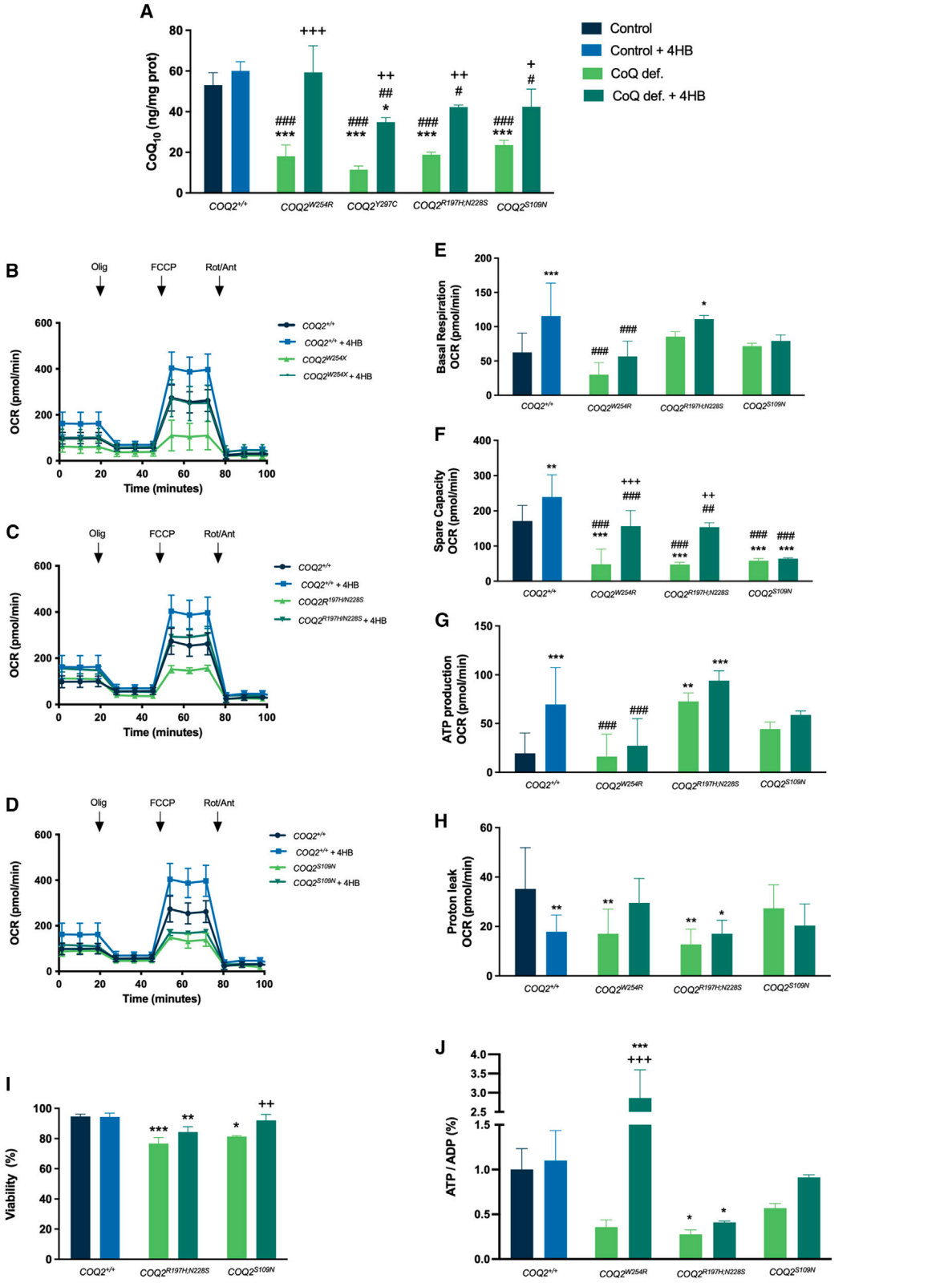

(legend on next page)

Stimulating endogenous CoQ biosynthesis could represent an alternative therapeutic approach with better outcomes than CoQ_{10} supplementation. In line with this strategy, administering 4HB could theoretically enhance COQ2 activity if the physiological concentration of 4HB is below the km, as recently suggested.[10] This approach may be relevant in pathogenic variants in *COQ2*, particularly if the mutated enzyme retains residual activity. Additionally, since HPDL is involved in 4HB synthesis[3] (Figure S1), supplementation of this compound could theoretically bypass the defect and rescue mitochondrial dysfunction in cells with *HPDL* pathogenic variants.[11]

Here, we demonstrate that 4HB normalizes CoQ biosynthesis in skin fibroblasts from patients with four different *COQ2* pathogenic variants, resulting in increased mitochondrial bioenergetics. Furthermore, we developed and characterized a mouse model with a homozygous *Coq2* pathogenic variant ($Coq2^{A252V}$) that exhibits multisystemic disease and perinatal lethality, mirroring clinical features observed in patients. Notably, 4HB therapy completely rescues the severe biochemical, metabolic, and morphological phenotype of $Coq2^{A252V}$ mice, providing a translatable and effective therapy for patients with primary CoQ deficiency and other mitochondrial diseases associated with secondary CoQ deficiency.

RESULTS

4HB normalizes CoQ levels and mitochondrial bioenergetics in skin fibroblasts with different pathogenic variants in *COQ2*

We initially investigated the potential therapeutic effects of 4HB supplementation in human skin fibroblasts obtained from patients exhibiting CoQ deficiency due to different pathogenic variants in *COQ2*, each associated with distinct clinical phenotypes (Table S1). Our results confirm CoQ_{10} deficiency in cells harboring different *COQ2* pathogenic variants (Figure 1A). Notably, 4HB supplementation partially normalizes CoQ_{10} levels in all four *COQ2* mutant cells (Figure 1A). Additionally, control cells exhibit a discernible trend toward increased CoQ_{10} levels when stimulated with 4HB (Figure 1A). The increase in CoQ_{10} levels is likely attributed to the upregulation of proteins involved in CoQ biosynthesis (Figure S2).

As a direct consequence of the augmented CoQ_{10} levels, mitochondrial respiration increases in both control and mutant cells, as illustrated in representative graphs from the Seahorse Mito-Stress assay (Figures 1B–1D). This enhancement is further supported by the resulting values of basal respiration (Figure 1E), spare capacity (Figure 1F), ATP production (Figure 1G), and proton leak (Figure 1H), although the latter has some variations that may reflect adaptations of the mitochondrial respiratory chain to conditions of low CoQ levels. In skin fibroblasts from a patient with an *HPDL* pathogenic variant, however, CoQ_{10} and CoQ_9 levels are comparable to those in control cells, and 4HB therapy does not increase CoQ_{10} levels (Figures S3A and S3B). Also, cell bioenergetics is not decreased in *HPDL* mutant cells, although 4HB therapy slightly increases mitochondrial respiration (Figures S3C and S3D).

The positive effects of 4HB supplementation in *COQ2* mutant cells extend to the increased viability of mutant cells grown in galactose medium (Figure 1I) and the elevation of the ATP/ADP ratio (Figure 1J). These findings corroborate the functional role of *de novo* CoQ_{10} in cellular performance and the oxidative phosphorylation (OxPhos) system. Collectively, these results provide a rationale for *in vivo* testing of 4HB therapy.

4HB stimulates CoQ biosynthesis *in vivo* and rescues the multisystemic phenotype and perinatal lethality of $Coq2^{A252V}$ mice

To investigate the pathophysiological consequences of *Coq2* defects *in vivo* and assess 4HB therapy, we generated a *Coq2* mutant mouse using homologous recombination to introduce a p.Ala252Val (A252V) (c.755C>T) pathogenic variant into mouse embryonic stem cells (see STAR Methods, Figure S7, and Data S1). The mouse mutation is homologous to the human p.Ala302Val (A302V) *COQ2* pathogenic variant previously described in two patients who were prematurely delivered by cesarean surgery due to fetal stress. These patients developed feeding problems, generalized edema, seizures, and apnea, leading to early death before 6 months of age.[12] Mating of heterozygous mice ($Coq2^{+/A252V}$) results in a normal Mendelian distribution during the embryonic development, but all $Coq2^{A252V}$ mice die between embryonic day (E) 16.5 and post-natal day 0 (Figure 2A). They exhibit an ostensible developmental delay and whitish appearance suggestive of a cardiovascular problem (Figures 2B, S4A, and S4B). This fatal phenotype is caused by a severe CoQ deficiency, as reflected in the levels of CoQ_9 in the brain and liver at E17.5 (Figures 2C, 2D, and S4E–S4L). Importantly, prenatal 4HB therapy completely rescues the perinatal lethality and developmental delay (Figures 2A, 2B, S4C, and S4D) of homozygous mice, most likely due to partial normalization of the CoQ_9 levels (Figures 2C, 2D, and S4E–S4L). The

Figure 1. Response of skin fibroblasts from patients with *COQ2* pathogenic variants to 4HB therapy

(A) CoQ_{10} levels (n = 4 in each experimental group).

(B–D) Representative graphs of Mito-Stress assays performed in the Seahorse XF^{24} bioanalyzer.

(E) Basal respiration.

(F) Spare capacity.

(G) ATP production.

(H) Proton leak (n = 4 in each experimental group).

(I) Cell viability (n = 4 in each experimental group).

(J) ATP/ADP ratio expressed by percentage of the control values (n = 4 in each experimental group).

4HB was used at a concentration of 1 mM, and the effects were evaluated after 7 days. Data are represented as mean ± SD. *p < 0.05 vs. $Coq2^{+/+}$; **p < 0.01 vs. $Coq2^{+/+}$; ***p < 0.001 vs. $Coq2^{+/+}$; #p < 0.05 vs. $Coq2^{+/+}$ treated with 4HB; ##p < 0.01 vs. $Coq2^{+/+}$ treated with 4HB; ###p < 0.001 vs. $Coq2^{+/+}$ treated with 4HB; +p < 0.05 vs. *Coq2* mutant; ++p < 0.05 vs. *Coq2* mutant; and +++p < 0.05 vs. *Coq2* mutant.

See also Figures S1–S3 and Table S1.

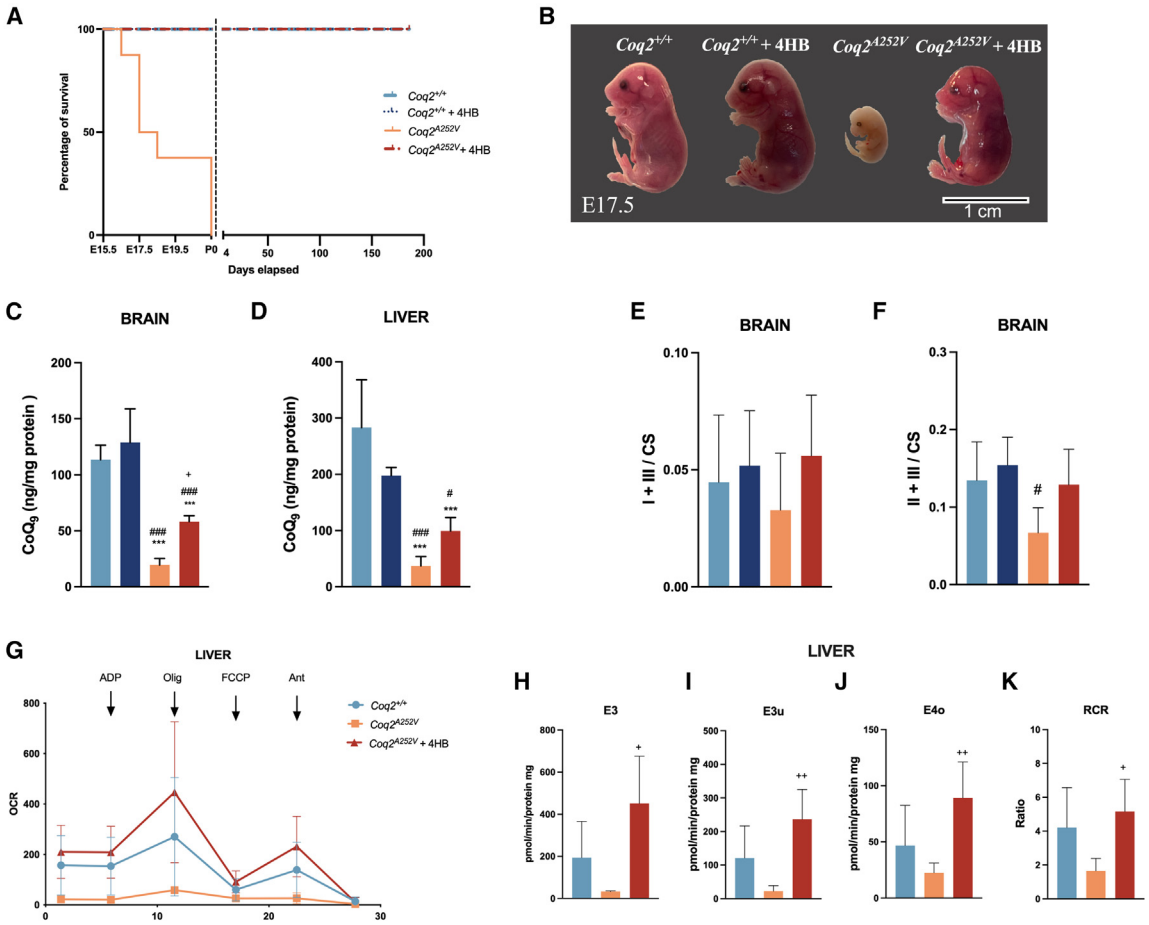

Figure 2. Effect of 4HB therapy on survival and mitochondrial function of *Coq2*^{A252V} mice

(A) Survival curve of mice from the experimental groups *Coq2*$^{+/+}$, *Coq2*$^{+/+}$ treated with 4HB, *Coq2*^{A252V}, and *Coq2*^{A252V} treated with 4HB (n = 10–12 in each experimental group).

(B) Representative photos of the embryos at E17.5.

(C and D) CoQ_9 levels in the brain (C) and liver (D) at E17.5 (n = 5 in each experimental group).

(E and F) CI+III (E) and CII+III (F) activities in the brain at E17.5 (n = 5 in each experimental group).

(G–K) Representative graph of the measurement of the oxygen consumption rate in isolated mitochondria from the liver at E17.5 (G) and quantification of state 3 (H), stage 3u (I), stage 4o (J), and respiratory control ratio (RCR) (K) of hepatic mitochondrial respiration (n = 4–6 in each experimental group).

4HB was given to the mice in the chow at a concentration of 0.33% (w/w). Scale bar: 1 cm (B). Data are represented as mean ± SD. ***$p < 0.001$ vs. *Coq2*$^{+/+}$; #$p < 0.05$ vs. *Coq2*$^{+/+}$ treated with 4HB; ###$p < 0.001$ vs. *Coq2*$^{+/+}$ treated with 4HB; +$p < 0.05$ vs. *Coq2*^{A252V}; and ++$p < 0.01$ vs. *Coq2*^{A252V}.

See also Figure S4.

variation in CoQ_9 levels correlates with the function of the OxPhos system. Specifically, *Coq2*^{A252V} mice show a trend toward decreased activities of the mitochondrial complex I+III (CI+III) and CII+III in the brain, and 4HB therapy rescues both activities (Figures 2E and 2F). Similarly, the livers of *Coq2*^{A252V} mice show a decrease in different stages of mitochondrial respiration (Figures 2G–2J), particularly at stage 3, and respiratory control ratio (Figure 2K), and 4HB therapy normalizes all parameters of mitochondrial respiration (Figures 2G–2K).

To further study the phenotype of the mouse model and the response to 4HB therapy, we first performed high-resolution episcopic microscopy analyses of embryos at E15.5. Remarkably, those analyses revealed that *Coq2*^{A252V} mice exhibit a delay in neurodevelopment, characterized by a diminished development of the telencephalon and a slight decrease in the volume of the lateral ventricles (Figures 3A–3F and S4M–S4T), compared to wild-type counterparts (Figures 3A–3F and S4M–S4T). Treatment with 4HB restores the normal developmental stage of the brain (Figures 3A–3F and S4M–S4T). The neurodevelopmental delay was further confirmed by MRI at E17.5 (Figures 3S–3U and S4U–S4W). Furthermore, *Coq2*^{A252V} mice show pericardial effusion and subcutaneous edema (Figure 3H), neither of which are observed in either wild-type (Figure 3G) or *Coq2*^{A252V} mice treated with 4HB (Figure 3I). The edema must be the consequence of cardiac insufficiency caused by the incomplete closure of the ventricular septum and the reduction in the thickness of the myocardium in *Coq2*^{A252V} mice (Figures 3M–3O) compared to wild-type embryos

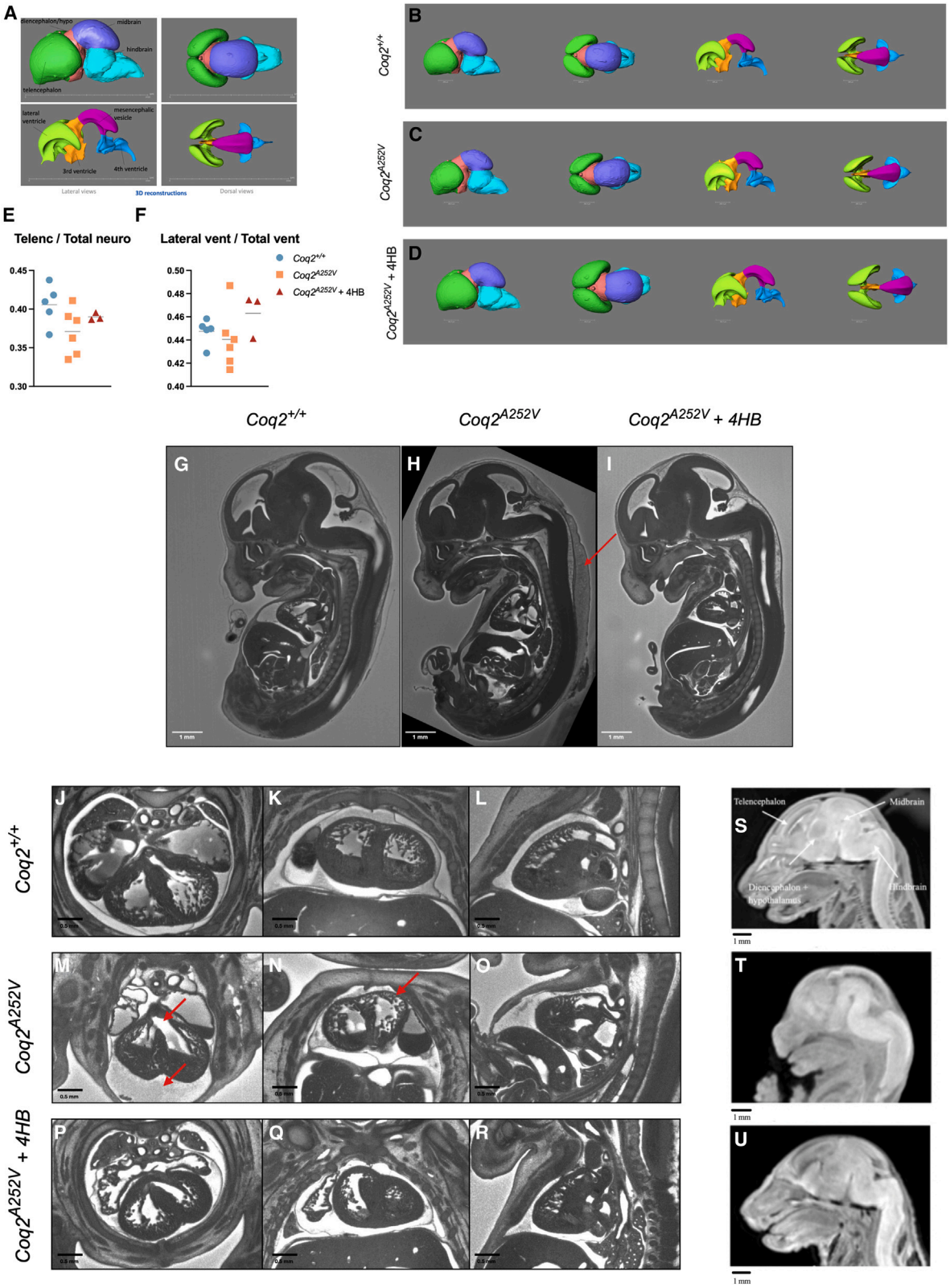

(legend on next page)

(Figures 3J–3L). 4HB therapy completely rescues the defect in cardiac development (Figures 3P–3R). Consequently, the volume of the cardiac ventricles increases in *Coq2*^{A252V} mice compared to *Coq2*$^{+/+}$ or *Coq2*^{A252V} mice treated with 4HB (Figures S4X–S4AA). The glomerular function does not seem to contribute to edema since the structure of the metanephros is normal and the total volume is unchanged between the groups (Figures S4AB–S4AD). To compare the results of 4HB with those under the standard treatment of oral CoQ_{10}, we also treated pregnant females with CoQ_{10}. So far, we got three littermates, with two born mutants. However, those mutants were clearly smaller in size than the other animals of the same littermates (Video S1), and they died between 7 and 28 days of age. Together, these results underscore the essential role of COQ2 protein, CoQ, and mitochondria in both cardiac and brain development during embryogenesis.[13,14] Notably, prenatal supplementation with 4HB can effectively alleviate the neurodevelopmental delay and cardiac insufficiency resulting from CoQ deficiency attributable to a defect in COQ2.

Chronic 4HB supplementation is safe and effective in maintaining physiological functions in young adult *Coq2*^{A252V} mice

Considering that 4HB therapy rescues the perinatal lethality of *Coq2*^{A252V} mice, we followed the treated animals and studied them at 1 month of age. *Coq2*^{A252V} mice treated with 4HB are physiognomically indistinguishable from *Coq2*$^{+/+}$ mice, whether treated or untreated, at 1 month of age, regardless the sex (Figures 4A–4C; Video S2). So far, we have treated mutant mice that have reached 7 months of age (Figure 2A), and they appear completely normal, both males (Video S3) and females (Video S3), as can be observed in these videos. The three experimental groups perform equally in the different tests used to evaluate the motor function (Figures 4D and S5A–S5D) at 1 month of age, and they weighed similar amounts (Figures 4E and 4F).

Morphologically, the brains of animals in the three experimental groups are normal on MRI (Figures 4G–4I), without any apparent lesions. This observation aligns with the absence of disparities in the neuron count within the cerebral cortex (Figures S6A–S6I), the quantity of myelin across assessed regions (Figures S6J–S6AA), and the number and morphology of Iba-1-labeled microglia (Figures S6AB–S6AS). While the count of astrocytes remains unchanged in most areas, there is an apparent increase in the cerebellum of 4HB-treated mutant mice (Figures S6AT–S6BU). Also, the structures of the heart and kidneys are similar in the three experimental groups (Figures 4J–4R). The absence of morphological abnormalities correlates with the functionality of the OxPhos system. The CoQ-dependent mitochondrial complexes' activities in the brain (Figures 4S–4T) and liver (Figures S5E and S5F), cerebral levels of lactate (Figures S5L–S5N), and mitochondrial respiration in the liver (Figures 4U–4Y) and kidney (Figures S5G–S5K) remain normalized in the treated mutant animals. Nevertheless, we observed that 4HB therapy stimulated the CoQ-dependent mitochondrial complexes' activities in the brain and liver (Figures 4S–4T, S5E, and S5F). Also, mitochondrial state 4 of respiration in the liver and kidney (Figures 4X and S5J) is increased in response to 4HB therapy, a CoQ-independent effect that needs further evaluation.

Since the major production of CoQ occurs in mitochondria, the results of the function of the OxPhos system must be influenced by CoQ_9 and CoQ_{10} levels, which were increased 2–3 times in the treated mutant animals during embryonic development. At 1 month of age, this increment remains stable. *Coq2*^{A252V} mice show 50%–60% of residual CoQ_9 and CoQ_{10} in the cerebrum, cerebellum, liver, and kidney (Figures 4Z–4AC and S5O–S5R), compared to *Coq2*$^{+/+}$ mice, and these residual levels seem to be sufficient to maintain the physiological functions of CoQ *in vivo*, as previously demonstrated in the *Coq9*^{Q95X} mouse model.[15] In the heart and skeletal muscle, 4HB therapy normalizes the levels of CoQ_9 and CoQ_{10} in *Coq2*^{A252V} mice (Figures 4AD–4AE and S5S–S5T). Interestingly, 4HB affects the production of both CoQ_9 and CoQ_{10}, so the CoQ_9/CoQ_{10} ratio remains normal in all tissues except the cerebellum and kidney, where the stimulation of CoQ_9 synthesis is superior to the stimulation of CoQ_{10} synthesis (Figures S5U–S5Z).

Suppression of 4HB supplementation in young adult *Coq2*^{A252V} mice leads to time- and tissue-specific declines in CoQ biosynthesis

To further elucidate the effects of 4HB therapy, we discontinued treatment in *Coq2*^{A252V} mice at 1 month of age and assessed the subsequent impact on phenotype and CoQ levels at different time points. The results show that, following the suppression of 4HB therapy during the next 16 days, *Coq2*^{A252V} mice were phenotypically indistinguishable from those under continuous 4HB therapy, as well as wild-type animals, as demonstrated by the results of body weight (Figures 5A and 5B), motor performance (Figures 5C–5E), and motor coordination (Figures 5F–5H). However, the suppression of 4HB negatively affects CoQ levels but with variations observed between tissues. Specifically, CoQ levels remain stable after 7 days of 4HB therapy suppression in the cerebrum and cerebellum (Figures 5I and 5J), while they decrease in the liver, kidney, heart, and skeletal muscle (Figures 5K–5N). After 20 days of

Figure 3. Morphological characterization of *Coq2*^{A252V} embryos and the response to 4HB therapy

(A–D) Representative high-resolution episcopic microscopy (HREM) images showing the 3D volume reconstruction of different areas of the brain and of ventricles of *Coq2*$^{+/+}$, *Coq2*^{A252V}, and *Coq2*^{A252V} treated with 4HB. Scale bars, 280 μm.

(E–F) Quantification of the volume of the telencephalon and lateral ventricle in embryos at E15.5 (n = 3–6 in each experimental group).

(G–I) Representative HREM images of the whole embryos *Coq2*$^{+/+}$ (G), *Coq2*^{A252V} (H), and *Coq2*^{A252V} treated with 4HB (I), showing the presence of edema in *Coq2*^{A252V} embryos (red arrow).

(J–R) Representative HREM images of the thoracic cavity of embryos *Coq2*$^{+/+}$ (J–L), *Coq2*^{A252V} (M–O), and *Coq2*^{A252V} treated with 4HB (P–R), showing the incomplete closure of the ventricular septum and the reduction in the thickness of the myocardium in *Coq2*^{A252V} mice. +$p < 0.05$ vs. *Coq2*^{A252V}.

(S–U) Representative MRI images of the brain of E17.5 embryos *Coq2*$^{+/+}$ (S), *Coq2*^{A252V} (T), and *Coq2*^{A262V} treated with 4HB (U) (n = 4 in each experimental group). 4HB was given to the mice in the chow at a concentration of 0.33% (w/w). Scale bars: 1 mm (G–I), 0.5 mm (J–R), and 1 mm (S–U).

See also Figure S4.

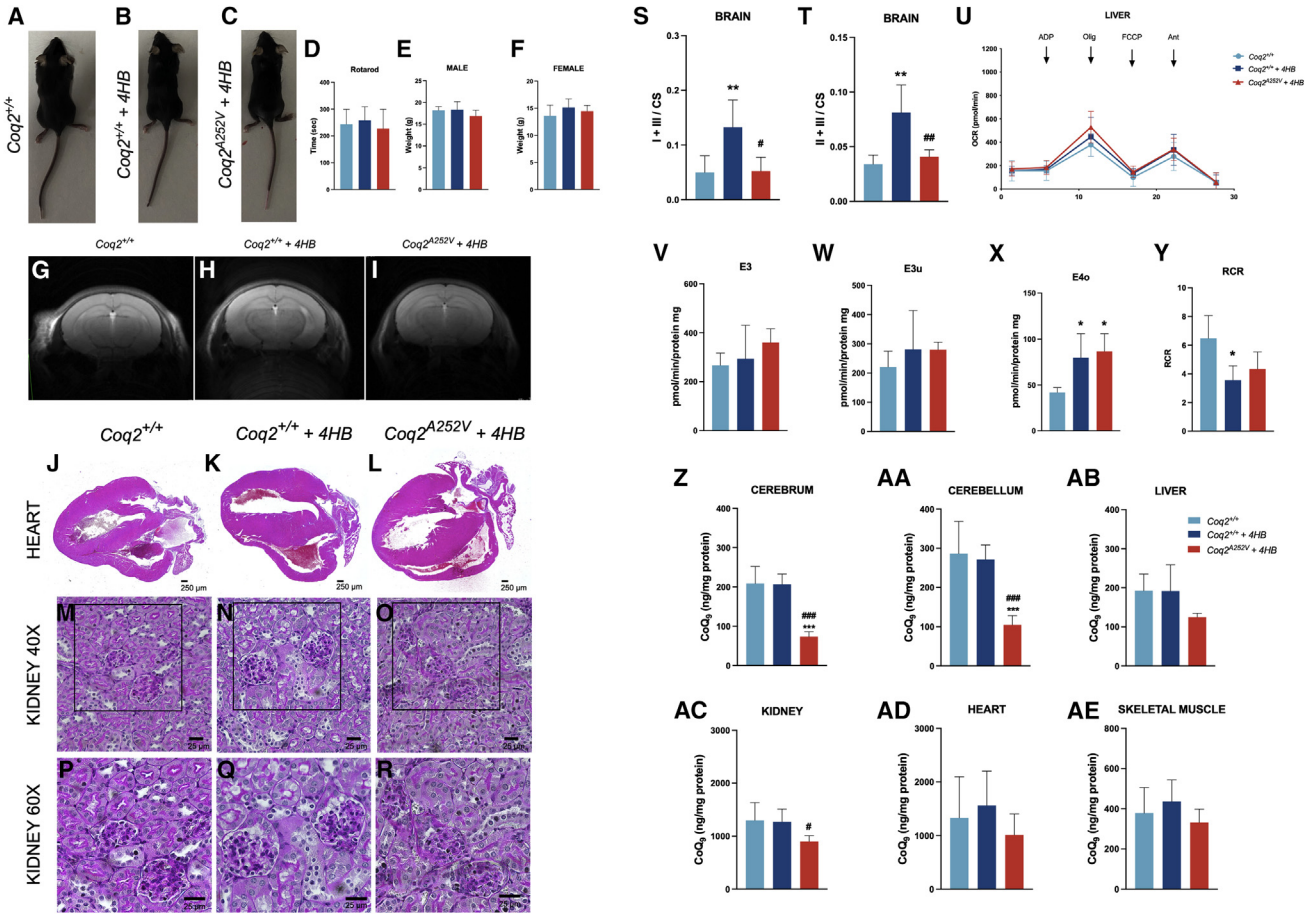

Figure 4. Characterization of *Coq2*^{A252V} mice treated with 4HB at 1 month of age

(A–C) Representative photos of the mice at 1 month of age.

(D) Rotarod test (n = 6–11 in each experimental group).

(E and F) Body weight of male (E) and female (F) mice (n = 8–14 in each experimental group).

(G–I) Magnetic resonance images of the diencephalon of mice of the experimental groups *Coq2*$^{+/+}$ (G), *Coq2*$^{+/+}$ (H) treated with 4HB, and *Coq2*^{A252V} (I) treated with 4HB (n = 3 in each experimental group).

(S–T) CoQ-dependent CI+III (S) and CII+III (T) activities in the brain (n = 5 in each experimental group).

(U–Y) Mitochondrial oxygen consumption rate in the liver showing a representation of an experiment involving the three experimental groups (U) and the quantifications of state 3 (V), state 3u (W), state 4o (X), and RCR (Y) (n = 4 in each experimental group).

(Z–AE) CoQ_9 levels in cerebrum (Z), cerebellum (AA), liver (AB), kidney (AC), heart (AD), and skeletal muscle (AF) (n = 6–11 in each experimental group).

4HB was given to the mice in the chow at a concentration of 0.33% (w/w). Scale bars: 250 μm (J–L) and 25 μm (M–R). Data are represented as mean ± SD. *p < 0.05 vs. *Coq2*$^{+/+}$; **p < 0.01 vs. *Coq2*$^{+/+}$; ***p < 0.001 vs. *Coq2*$^{+/+}$; #p < 0.05 vs. *Coq2*$^{+/+}$ treated with 4HB; ##p < 0.01 vs. *Coq2*$^{+/+}$ treated with 4HB; and ###p < 0.001 vs. *Coq2*$^{+/+}$ treated with 4HB.

See also Figures S5 and S6.

suppression of 4HB therapy, CoQ levels slightly decrease in the cerebrum and cerebellum (Figures 5I and 5J), and they further decrease in the liver, kidney, heart, and skeletal muscle (Figures 5K–5N). Nevertheless, except in the liver, the residual CoQ levels are maintained in the range of 25%–40% of the control values. This observation may explain the absence of phenotypic effects during this relatively short period. Overall, these data suggest that the functions of the CoQ biosynthetic pathway may differ between the embryonic and post-natal periods, with tissue-specific differences. Pathogenic variants in *Coq2* may exert more intense pathophysiological consequences during embryonic development.

DISCUSSION

CoQ deficiency syndrome represents a mitochondrial disorder known for its clinical heterogeneity and limited responsiveness to conventional CoQ_{10}-based therapy. Our investigation demonstrates that substrate enhancement therapy, which involves elevating levels of the precursor for CoQ biosynthesis, and the COQ2 substrate, specifically 4HB, robustly activates endogenous CoQ biosynthesis in both *in vitro* and *in vivo* models of CoQ deficiency associated with *COQ2* pathogenic variants. This intervention effectively ameliorates the observed biochemical and morphological abnormalities, leading to the rescue of

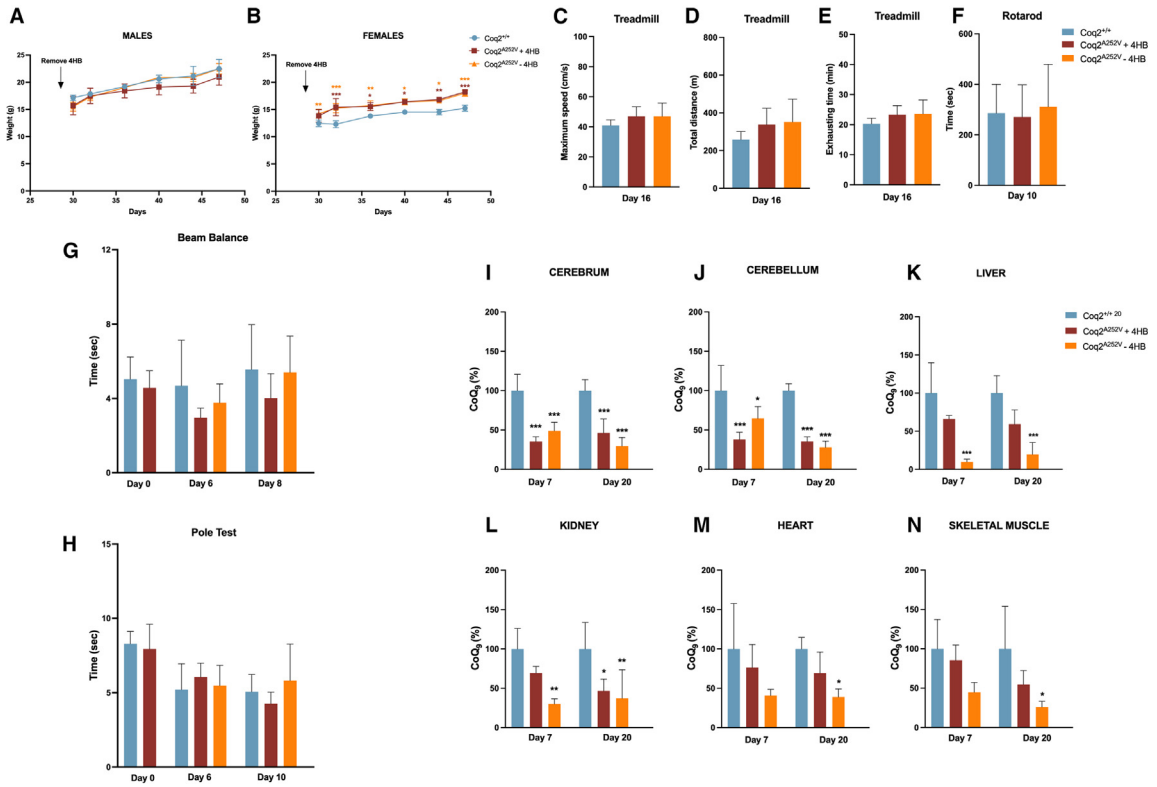

Figure 5. Phenotypic and metabolic evaluation after suppression of 4HB therapy in young adult *Coq*^{A252V}mice

(A and B) Body weight of male (A) and female (B) mice (n = 5–9 in each experimental group).

(C–E) Treadmill test at day 16 after the suppression of 4HB therapy, with quantifications of maximum speed (C), total distance (D), and exhausting time (E) (n = 5 in each experimental group).

(F) Rotarod test at day 10 after the suppression of 4HB therapy (n = 5 in each experimental group).

(G) Beam balance test at days 2, 6, and 10 after the suppression of 4HB therapy (n = 5 in each experimental group).

(H) Pole test at days 2, 6, and 10 after the suppression 4HB therapy (n = 5 in each experimental group).

(I–N) CoQ_9 levels at days 7 and 20 after the suppression of 4HB in the cerebrum (I), cerebellum (J), liver (K), kidney (L), heart (M), and skeletal muscle (N) (n = 5 in each experimental group).

4HB was given to the mice in the chow at a concentration of 0.33% (w/w). Data are represented as mean ± SD. *p < 0.05 vs. *Coq2*$^{+/+}$; **p < 0.01 vs. *Coq2*$^{+/+}$; ***p < 0.001 vs. *Coq2*$^{+/+}$; #p < 0.05 vs. *Coq2*$^{+/+}$ treated with 4HB; ##p < 0.01 vs. *Coq2*$^{+/+}$ treated with 4HB; and ###p < 0.001 vs. *Coq2*$^{+/+}$ treated with 4HB.

perinatal lethality and resulting in lifespans similar to those of wild-type animals.

Conventional treatment entails supplementing with exogenous CoQ_{10}; however, its effectiveness is hindered by poor absorption and bioavailability, attributed to the high lipophilicity of the polyprenoid tail,[16] and the subsequent inadequate delivery to the mitochondria,[9] the site of CoQ_{10}'s metabolic activity.[1] To address this limitation, we have investigated a strategy to elevate mitochondrial CoQ levels by stimulating the endogenous CoQ biosynthetic pathway through 4HB supplementation. Through 4HB therapy, we observed a partial rescue of CoQ levels in skin fibroblasts obtained from patients with various *COQ2* pathogenic variants, as well as in a *Coq2*-mutated mouse model. *De novo* CoQ generated through 4HB stimulation exhibits functionality within the mitochondrial respiratory chain, evidenced by heightened mitochondrial respiration, CoQ-dependent complex activities, and ATP/ADP ratio. Consequently, 4HB therapy not only mitigates cell death *in vitro* but also rescues multisystemic disease *in vivo*, surpassing the therapeutic effects of exogenous CoQ_{10} supplementation. Therefore, this 4HB-based substrate enhancement therapy has proven successful in two preclinical models, (1) the new *Coq2*-mutated mouse model mirroring a pathogenic variant found in patients with the multisystemic disease variant of CoQ deficiency, in which 4HB therapy fully rescues the fatal phenotype by normalizing CoQ levels and improving mitochondrial bioenergetics, and (2) skin fibroblasts obtained from patients with diverse *COQ2* pathogenic variants, providing evidence for its potential efficacy against *COQ2* defects in humans irrespective of the specific pathogenic variant and clinical presentation (Table S1).[17]

The superior outcomes of 4HB over CoQ_{10} can be attributed to its favorable bioavailability, its capacity to increase intramitochondrial CoQ levels, and its ability to increase both CoQ_9 and CoQ_{10}, maintaining a balanced CoQ_9/CoQ_{10} ratio.[10] Although the biological significance of having ubiquinone with different sizes of the polyprenoid tail is uncertain, the CoQ_9/CoQ_{10} ratio notably varies between tissues in rodents and human.[18,19] This

observation suggests that the production of both ubiquinone species is regulated in a tissue-specific manner, aligning with their distinct physiological functions in each tissue. Regardless, the distinctions in the therapeutic effects of 4HB and CoQ_{10} are significant for potential clinical translation, particularly considering the poor responsiveness of patients with *COQ2* pathogenic variants to exogenous CoQ_{10} supplementation.[17]

The tissue specificities in CoQ biosynthesis are evident in the response of the brain and liver during embryogenesis to 4HB supplementation. Assuming that the concentration of 4HB is lower than its km for COQ2,[10] an increase in the 4HB concentration is expected to elevate the COQ2 reaction rate, influencing CoQ levels. This phenomenon is observed in the brain of both $Coq2^{+/+}$ and $Coq2^{A252V}$ embryos and in the liver of $Coq2^{A252V}$ embryos. However, 4HB appears to slightly decrease CoQ levels in the liver of $Coq2^{+/+}$ embryos, suggesting that an excess of 4HB or its catabolized metabolites may induce substrate inhibition of COQ2 if its km and/or Vmax are not modified.[20] Nonetheless, this mild inhibitory effect is not observed in young adult animals, likely due to the decrease in the dose as a consequence of the animals' growth.

An additional intriguing finding from this study is that 4HB therapy can be employed in pregnant females, indicating that 4HB can traverse both the blood-placental barrier and the blood-brain barrier, and it can be passed on to offspring through breast milk. These data underscore the compound's safety profile. Furthermore, it is noteworthy that after cessation of 4HB therapy, residual CoQ levels were maintained within the range of 25%–40% of control values. These levels surpass those observed during embryonic development. Thus, the A252V pathogenic variant in *Coq2* appears to have a more severe impact during embryonic development than in young adult mice. This observation may reflect disparities in endogenous 4HB and CoQ metabolism during these developmental periods.[21] The absence of a severe phenotype with 40% residual CoQ levels was previously demonstrated in the $Coq9^{Q95X}$ murine model,[15] although a more extensive evaluation over longer periods in the $Coq2^{A252V}$ murine model must be undertaken. In fact, the phenotypes become evident after longer periods in other mouse models with primary CoQ deficiency resulting from mutations in *Pdss2*, *Coq8a*, or *Coq9*.[22–24]

While specifically designed for severe CoQ deficiency due to the *COQ2* pathogenic variant, our study suggests potential benefits for other CoQ deficiency cases, including HPDL pathogenic variants. Although results in skin fibroblasts from a patient with an HPDL pathogenic variant are inconclusive, indicating no significant effects, the existence of an HPDL-independent pathway for 4HB synthesis implies distinct roles in dividing vs. non-dividing cells,[3] necessitating further evaluation in organoids and animal models of HPDL deficiency.[25] Additionally, multiple system atrophy emerges (MSA) as another potential target disease for 4HB therapy, given its association with CoQ deficiency, both with and without *COQ2* variants.[26–28] Furthermore, other diseases where secondary CoQ deficiency has been reported could be potentially treated by 4HB supplementation.[29–31]

Successful strategies modulating endogenous CoQ biosynthesis have been reported in other preclinical models using the 4HB analogs β-resorcylic acid (β-RA = 2,4-dihydroxybenzoic acid) and vanillic acid.[32] In these cases, therapeutic effects are attributed to (1) a bypass mechanism that partially increases CoQ levels in defects in *COQ6*[33,34] and reduces the accumulation of a toxic intermediate metabolite of the CoQ biosynthetic pathway in cases of defects in *Coq7* and *Coq9*,[15,35–40] (2) an up-regulation of COQ4 in cells and tissues with pathogenic variants in *COQ9*,[39,40] and (3) unclear β-RA-induced mechanisms leading to the rescue of the nephrotic phenotype in podocyte-specific *Coq6* or *Adck4* knockout mice.[41,42] These findings collectively suggest that 4HB and its analogs can effectively treat CoQ deficiencies, but each analog must be specifically tailored for pathogenic variants in particular genes. Furthermore, 4HB therapy stands out as the only one based on enhancing the residual activity of a defective enzyme in the CoQ biosynthetic pathway.

In conclusion, 4HB therapy emerges as an effective and safe *in vivo* treatment for CoQ deficiency linked to *COQ2* pathogenic variants, showcasing potential translational applicability to other diseases involving *COQ2* variants (e.g., MSA) and cases of secondary CoQ deficiency. This substrate enhancement therapy marks a noteworthy advancement in the realm of mitochondrial medicine.

Limitations of the study

While our study highlights robust therapeutic effects both *in vitro* within human cells and *in vivo* using a murine model, we acknowledge several considerations that should be taken into account before contemplating the potential translation of this therapy into clinical applications: (1) the translation of the mouse dose to its human equivalent needs careful consideration, accounting for various factors such as compound metabolization and differences in body surface area; (2) assessing the therapy's long-term effects is imperative, encompassing not only therapeutic outcomes but also potential toxicity that may manifest over extended periods; (3) since the $Coq2^{A252V}$ model shows perinatal lethality, we treated pregnant females to prevent the onset of the disease, but we do not know the effects of the supplementation after disease onset. This is particularly relevant as CoQ deficiency due to *COQ2* pathogenic variants is usually diagnosed in childhood. Finally, (4) our findings suggest variations in CoQ metabolism at different ages, conditions, and tissues. The adaptive nature of the CoQ biosynthetic pathway during animal development raises the possibility of critical moments that may influence outcomes. Further investigation is warranted to elucidate these mechanistic aspects.

STAR★METHODS

Detailed methods are provided in the online version of this paper and include the following:

- KEY RESOURCES TABLE
- RESOURCES AVAILABILITY
  - Lead contact
  - Materials availability
  - Data and code availability
- EXPERIMENTAL MODEL AND STUDY PARTICIPANT DETAILS
  - Human skin fibroblasts
  - Generation of the $Coq2^{A252V}$ mouse model
- METHOD DETAILS
  - Cell culture and treatment
  - Treatment in mice

- Mouse phenotyping
- Quantification of CoQ_9 and CoQ_{10} levels
- Assessment of mitochondrial respiration
- Assessment of CoQ-dependent respiratory chain activities
- Measurement of adenosine nucleotides levels
- Assessment of cell death
- Histology and immunohistochemistry
- High-resolution episcopic microscopy (HREM)
- *In vivo* MRI and proton MRS

● QUANTIFICATION AND STATISTICAL ANALYSIS

SUPPLEMENTAL INFORMATION

Supplemental information can be found online at https://doi.org/10.1016/j.celrep.2024.114148.

ACKNOWLEDGMENTS

The authors thank Dr. Inna Inashkina (Latvian Biomedical Research and Study Center) for providing the skin fibroblasts of the patient with the *HPDL* pathogenic variant and Dr. Marisa García-Martín for the technical support in the MRI studies. This work was supported by the grants PID2021-126788OB-I00 from the MICIU/AEI/10.13039/501100011033, Spain, and the ERDF/EU; MDA-602322 from the Muscular Dystrophy Association; and PEER-0083-2020 from the Junta de Andalucía. J.C.-S. and L.J.-S. were supported by the Consejería de Salud, Junta de Andalucía, Spain. J.M.M.-G. was supported by the "Margarita Salas program" from the Ministerio de Universidades, Spain. P.G.-G. was supported by University of Granada. S.L.-H. was supported by the "FPU program" from the Ministerio de Universidades, Spain. C.M.Q. is supported by DOD grant W81XWH2010807 and NIH grants R21AG077243-01A1 and 1R01NS134902-01. The authors are also thankful for the support of the Unit of Excellence "UNETE" from the University of Granada (UCE-PP2017-05). The results shown in this article will constitute a section of J.C.-S.'s doctoral thesis at the University of Granada.

AUTHOR CONTRIBUTIONS

Conceptualization, L.C.L., C.M.Q., and J.C.-S.; methodology, J.C.-S., J.M.M.-G., P.G.-G., O.W., L.J.-S., S.L.-H., and M.E.D.-C.; software, J.C.-S., J.M.M.-G., P.G.-G., and O.W.; investigation, J.C.-S., J.M.M.-G., and P.G.-G.; writing – original draft, J.C.-S. and L.C.L.; writing – review & editing, all authors; visualization, J.C.-S. and J.M.M.-G.; supervision, L.C.L.; funding acquisition, C.M.Q. and L.C.L.

DECLARATION OF INTERESTS

J.C.-S., J.M.M.-G., P.G.-G., L.J.-S., M.E.D.-C., S.L.-H., and L.C.L. are inventors listed on the patent "Compound to stimulate mitochondrial metabolism in gametes and embryos" filed in Spain on February 28, 2024 (application number P202430145).

Received: January 11, 2024
Revised: March 3, 2024
Accepted: April 9, 2024
Published: May 1, 2024

REFERENCES

1. Hidalgo-Gutiérrez, A., González-García, P., Díaz-Casado, M.E., Barriocanal-Casado, E., López-Herrador, S., Quinzii, C.M., and López, L.C. (2021). Metabolic Targets of Coenzyme Q10 in Mitochondria. Antioxidants *10*, 520. https://doi.org/10.3390/antiox10040520.
2. Guerra, R.M., and Pagliarini, D.J. (2023). Coenzyme Q biochemistry and biosynthesis. Trends Biochem. Sci. *48*, 463–476. https://doi.org/10.1016/j.tibs.2022.12.006.
3. Banh, R.S., Kim, E.S., Spillier, Q., Biancur, D.E., Yamamoto, K., Sohn, A.S.W., Shi, G., Jones, D.R., Kimmelman, A.C., and Pacold, M.E. (2021). The polar oxy-metabolome reveals the 4-hydroxymandelate CoQ10 synthesis pathway. Nature *597*, 420–425. https://doi.org/10.1038/s41586-021-03865-w.
4. Pelosi, L., Morbiato, L., Burgardt, A., Tonello, F., Bartlett, A.K., Guerra, R.M., Ferizhendi, K.K., Desbats, M.A., Rascalou, B., Marchi, M., et al. (2024). COQ4 is required for the oxidative decarboxylation of the C1 carbon of coenzyme Q in eukaryotic cells. Mol. Cell *84*, 981–989.e7. https://doi.org/10.1016/j.molcel.2024.01.003.
5. Fernández-Del-Río, L., Nag, A., Gutiérrez Casado, E., Ariza, J., Awad, A.M., Joseph, A.I., Kwon, O., Verdin, E., de Cabo, R., Schneider, C., et al. (2017). Kaempferol increases levels of coenzyme Q in kidney cells and serves as a biosynthetic ring precursor. Free Radic. Biol. Med. *110*, 176–187. https://doi.org/10.1016/j.freeradbiomed.2017.06.006.
6. Alcázar-Fabra, M., Rodríguez-Sánchez, F., Trevisson, E., and Brea-Calvo, G. (2021). Primary Coenzyme Q deficiencies: A literature review and online platform of clinical features to uncover genotype-phenotype correlations. Free Radic. Biol. Med. *167*, 141–180. https://doi.org/10.1016/j.freeradbiomed.2021.02.046.
7. Wiessner, M., Maroofian, R., Ni, M.Y., Pedroni, A., Müller, J.S., Stucka, R., Beetz, C., Efthymiou, S., Santorelli, F.M., Alfares, A.A., et al. (2021). Biallelic variants in HPDL cause pure and complicated hereditary spastic paraplegia. Brain *144*, 1422–1434. https://doi.org/10.1093/brain/awab041.
8. Wang, Y., and Hekimi, S. (2022). The efficacy of coenzyme Q10 treatment in alleviating the symptoms of primary coenzyme Q10 deficiency: A systematic review. J. Cell Mol. Med. *26*, 4635–4644. https://doi.org/10.1111/jcmm.17488.
9. Bentinger, M., Dallner, G., Chojnacki, T., and Swiezewska, E. (2003). Distribution and breakdown of labeled coenzyme Q10 in rat. Free Radic. Biol. Med. *34*, 563–575.
10. Pierrel, F. (2017). Impact of Chemical Analogs of 4-Hydroxybenzoic Acid on Coenzyme Q Biosynthesis: From Inhibition to Bypass of Coenzyme Q Deficiency. Front. Physiol. *8*, 436. https://doi.org/10.3389/fphys.2017.00436.
11. Sun, Y., Wei, X., Fang, F., Shen, Y., Wei, H., Li, J., Ye, X., Zhan, Y., Ye, X., Liu, X., et al. (2021). HPDL deficiency causes a neuromuscular disease by impairing the mitochondrial respiration. J Genet Genomics *48*, 727–736. https://doi.org/10.1016/j.jgg.2021.01.009.
12. Jakobs, B.S., van den Heuvel, L.P., Smeets, R.J.P., de Vries, M.C., Hien, S., Schaible, T., Smeitink, J.A.M., Wevers, R.A., Wortmann, S.B., and Rodenburg, R.J.T. (2013). A novel mutation in COQ2 leading to fatal infantile multisystem disease. J. Neurol. Sci. *326*, 24–28. https://doi.org/10.1016/j.jns.2013.01.004.
13. Zhao, Q., Sun, Q., Zhou, L., Liu, K., and Jiao, K. (2019). Complex Regulation of Mitochondrial Function During Cardiac Development. J. Am. Heart Assoc. *8*, e012731. https://doi.org/10.1161/JAHA.119.012731.
14. Oyarzábal, A., Musokhranova, U., Barros, L.F., and García-Cazorla, A. (2021). Energy metabolism in childhood neurodevelopmental disorders. EBioMedicine *69*, 103474, ARTN. https://doi.org/10.1016/j.ebiom.2021.103474.
15. Luna-Sánchez, M., Díaz-Casado, E., Barca, E., Tejada, M.Á., Montilla-García, Á., Cobos, E.J., Escames, G., Acuña-Castroviejo, D., Quinzii, C.M., and López, L.C. (2015). The clinical heterogeneity of coenzyme Q10 deficiency results from genotypic differences in the Coq9 gene. EMBO Mol. Med. *7*, 670–687. https://doi.org/10.15252/emmm.201404632.
16. García-Corzo, L., Luna-Sánchez, M., Doerrier, C., Ortiz, F., Escames, G., Acuña-Castroviejo, D., and López, L.C. (2014). Ubiquinol-10 ameliorates mitochondrial encephalopathy associated with CoQ deficiency. Biochim. Biophys. Acta *1842*, 893–901. https://doi.org/10.1016/j.bbadis.2014.02.008.
17. Herebian, D., Seibt, A., Smits, S.H.J., Rodenburg, R.J., Mayatepek, E., and Distelmaier, F. (2017). 4-Hydroxybenzoic acid restores CoQ(10) biosynthesis in human COQ2 deficiency. Ann. Clin. Transl. Neurol. *4*, 902–908. https://doi.org/10.1002/acn3.486.

18. Aberg, F., Appelkvist, E.L., Dallner, G., and Ernster, L. (1992). Distribution and redox state of ubiquinones in rat and human tissues. Arch. Biochem. Biophys. *295*, 230–234. https://doi.org/10.1016/0003-9861(92)90511-t.

19. Parrado-Fernández, C., López-Lluch, G., Rodríguez-Bies, E., Santa-Cruz, S., Navas, P., Ramsey, J.J., and Villalba, J.M. (2011). Calorie restriction modifies ubiquinone and COQ transcript levels in mouse tissues. Free Radic. Biol. Med. *50*, 1728–1736.

20. Nishida, I., Yanai, R., Matsuo, Y., Kaino, T., and Kawamukai, M. (2020). Benzoic acid inhibits Coenzyme Q biosynthesis in Schizosaccharomyces pombe. PLoS One *15*, e0242616. https://doi.org/10.1371/journal.pone.0242616.

21. Turunen, M., Olsson, J., and Dallner, G. (2004). Metabolism and function of coenzyme Q. Biochim. Biophys. Acta *1660*, 171–199.

22. Peng, M., Falk, M.J., Haase, V.H., King, R., Polyak, E., Selak, M., Yudkoff, M., Hancock, W.W., Meade, R., Saiki, R., et al. (2008). Primary coenzyme Q deficiency in Pdss2 mutant mice causes isolated renal disease. PLoS Genet. *4*, e1000061.

23. Stefely, J.A., Licitra, F., Laredj, L., Reidenbach, A.G., Kemmerer, Z.A., Grangeray, A., Jaeg-Ehret, T., Minogue, C.E., Ulbrich, A., Hutchins, P.D., et al. (2016). Cerebellar Ataxia and Coenzyme Q Deficiency through Loss of Unorthodox Kinase Activity. Mol. Cell *63*, 608–620. https://doi.org/10.1016/j.molcel.2016.06.030.

24. García-Corzo, L., Luna-Sánchez, M., Doerrier, C., García, J.A., Guarás, A., Acín-Pérez, R., Bullejos-Peregrín, J., López, A., Escames, G., Enríquez, J.A., et al. (2013). Dysfunctional Coq9 protein causes predominant encephalomyopathy associated with CoQ deficiency. Hum. Mol. Genet. *22*, 1233–1248. https://doi.org/10.1093/hmg/dds530.

25. Ghosh, S.G., Lee, S., Fabunan, R., Chai, G., Zaki, M.S., Abdel-Salam, G., Sultan, T., Ben-Omran, T., Alvi, J.R., McEvoy-Venneri, J., et al. (2021). Biallelic variants in HPDL, encoding 4-hydroxyphenylpyruvate dioxygenase-like protein, lead to an infantile neurodegenerative condition. Genet. Med. *23*, 524–533. https://doi.org/10.1038/s41436-020-01010-y.

26. Multiple-System Atrophy Research Collaboration (2013). Mutations in COQ2 in familial and sporadic multiple-system atrophy. N. Engl. J. Med. *369*, 233–244. https://doi.org/10.1056/NEJMoa1212115.

27. Barca, E., Kleiner, G., Tang, G., Ziosi, M., Tadesse, S., Masliah, E., Louis, E.D., Faust, P., Kang, U.J., Torres, J., et al. (2016). Decreased Coenzyme Q10 Levels in Multiple System Atrophy Cerebellum. J. Neuropathol. Exp. Neurol. *75*, 663–672. https://doi.org/10.1093/jnen/nlw037.

28. Nakamoto, F.K., Okamoto, S., Mitsui, J., Sone, T., Ishikawa, M., Yamamoto, Y., Kanegae, Y., Nakatake, Y., Imaizumi, K., Ishiura, H., et al. (2018). The pathogenesis linked to coenzyme Q10 insufficiency in iPSC-derived neurons from patients with multiple-system atrophy. Sci. Rep. *8*, 14215. https://doi.org/10.1038/s41598-018-32573-1.

29. Kühl, I., Miranda, M., Atanassov, I., Kuznetsova, I., Hinze, Y., Mourier, A., Filipovska, A., and Larsson, N.G. (2017). Transcriptomic and proteomic landscape of mitochondrial dysfunction reveals secondary coenzyme Q deficiency in mammals. Elife *6*, e30952. https://doi.org/10.7554/eLife.30952.

30. Fazakerley, D.J., Chaudhuri, R., Yang, P., Maghzal, G.J., Thomas, K.C., Krycer, J.R., Humphrey, S.J., Parker, B.L., Fisher-Wellman, K.H., Meoli, C.C., et al. (2018). Mitochondrial CoQ deficiency is a common driver of mitochondrial oxidants and insulin resistance. Elife *7*, e32111. https://doi.org/10.7554/eLife.32111.

31. Navas, P., Cascajo, M.V., Alcázar-Fabra, M., Hernández-Camacho, J.D., Sánchez-Cuesta, A., Rodríguez, A.B.C., Ballesteros-Simarro, M., Arroyo-Luque, A., Rodríguez-Aguilera, J.C., Fernández-Ayala, D.J.M., et al. (2021). Secondary CoQ10 deficiency, bioenergetics unbalance in disease and aging. Biofactors *47*, 551–569. https://doi.org/10.1002/biof.1733.

32. González-García, P., Barriocanal-Casado, E., Díaz-Casado, M.E., López-Herrador, S., Hidalgo-Gutiérrez, A., and López, L.C. (2021). Animal Models of Coenzyme Q Deficiency: Mechanistic and Translational Learnings. Antioxidants *10*, 1687. https://doi.org/10.3390/antiox10111687.

33. Acosta Lopez, M.J., Trevisson, E., Canton, M., Vazquez-Fonseca, L., Morbidoni, V., Baschiera, E., Frasson, C., Pelosi, L., Rascalou, B., Desbats, M.A., et al. (2019). Vanillic Acid Restores Coenzyme Q Biosynthesis and ATP Production in Human Cells Lacking COQ6. Oxid. Med. Cell. Longev. *2019*, 3904905. https://doi.org/10.1155/2019/3904905.

34. Doimo, M., Trevisson, E., Airik, R., Bergdoll, M., Santos-Ocaña, C., Hildebrandt, F., Navas, P., Pierrel, F., and Salviati, L. (2014). Effect of vanillic acid on COQ6 mutants identified in patients with coenzyme Q deficiency. Biochim. Biophys. Acta *1842*, 1–6. https://doi.org/10.1016/j.bbadis.2013.10.007.

35. Wang, Y., Smith, C., Parboosingh, J.S., Khan, A., Innes, M., and Hekimi, S. (2017). Pathogenicity of two COQ7 mutations and responses to 2,4-dihydroxybenzoate bypass treatment. J. Cell Mol. Med. *21*, 2329–2343. https://doi.org/10.1111/jcmm.13154.

36. Wang, Y., Oxer, D., and Hekimi, S. (2015). Mitochondrial function and lifespan of mice with controlled ubiquinone biosynthesis. Nat. Commun. *6*, 6393. https://doi.org/10.1038/ncomms7393.

37. Hidalgo-Gutiérrez, A., Barriocanal-Casado, E., Díaz-Casado, M.E., González-García, P., Zenezini Chiozzi, R., Acuña-Castroviejo, D., and López, L.C. (2021). beta-RA Targets Mitochondrial Metabolism and Adipogenesis, Leading to Therapeutic Benefits against CoQ Deficiency and Age-Related Overweight. Biomedicines *9*, 1457. https://doi.org/10.3390/biomedicines9101457.

38. Hidalgo-Gutiérrez, A., Barriocanal-Casado, E., Bakkali, M., Díaz-Casado, M.E., Sánchez-Maldonado, L., Romero, M., Sayed, R.K., Prehn, C., Escames, G., Duarte, J., et al. (2019). beta-RA reduces DMQ/CoQ ratio and rescues the encephalopathic phenotype in Coq9(R239X) mice. EMBO Mol. Med. *11*, e9466. https://doi.org/10.15252/emmm.201809466.

39. González-García, P., Díaz-Casado, M.E., Hidalgo-Gutiérrez, A., Jiménez-Sánchez, L., Bakkali, M., Barriocanal-Casado, E., Escames, G., Chiozzi, R.Z., Völlmy, F., Zaal, E.A., et al. (2022). The Q-junction and the inflammatory response are critical pathological and therapeutic factors in CoQ deficiency. Redox Biol. *55*, 102403. https://doi.org/10.1016/j.redox.2022.102403.

40. Herebian, D., Seibt, A., Smits, S.H.J., Bünning, G., Freyer, C., Prokisch, H., Karall, D., Wredenberg, A., Wedell, A., López, L.C., et al. (2017). Detection of 6-demethoxyubiquinone in CoQ10 deficiency disorders: Insights into enzyme interactions and identification of potential therapeutics. Mol. Genet. Metabol. *121*, 216–223. https://doi.org/10.1016/j.ymgme.2017.05.012.

41. Widmeier, E., Airik, M., Hugo, H., Schapiro, D., Wedel, J., Ghosh, C.C., Nakayama, M., Schneider, R., Awad, A.M., Nag, A., et al. (2019). Treatment with 2,4-Dihydroxybenzoic Acid Prevents FSGS Progression and Renal Fibrosis in Podocyte-Specific Coq6 Knockout Mice. J. Am. Soc. Nephrol. *30*, 393–405. https://doi.org/10.1681/ASN.2018060625.

42. Widmeier, E., Yu, S., Nag, A., Chung, Y.W., Nakayama, M., Fernández-Del-Río, L., Hugo, H., Schapiro, D., Buerger, F., Choi, W.I., et al. (2020). ADCK4 Deficiency Destabilizes the Coenzyme Q Complex, Which Is Rescued by 2,4-Dihydroxybenzoic Acid Treatment. J. Am. Soc. Nephrol. *31*, 1191–1211. https://doi.org/10.1681/ASN.2019070756.

43. Robinson, B.H., Petrova-Benedict, R., Buncic, J.R., and Wallace, D.C. (1992). Nonviability of cells with oxidative defects in galactose medium: a screening test for affected patient fibroblasts. Biochem. Med. Metab. Biol. *48*, 122–126.

44. López, L.C., Quinzii, C.M., Area, E., Naini, A., Rahman, S., Schuelke, M., Salviati, L., DiMauro, S., and Hirano, M. (2010). Treatment of CoQ(10) deficient fibroblasts with ubiquinone, CoQ analogs, and vitamin C: time- and compound-dependent effects. PLoS One *5*, e11897.

45. Quinzii, C.M., López, L.C., Von-Moltke, J., Naini, A., Krishna, S., Schuelke, M., Salviati, L., Navas, P., DiMauro, S., and Hirano, M. (2008). Respiratory chain dysfunction and oxidative stress correlate with severity of primary CoQ10 deficiency. Faseb. J. *22*, 1874–1885.

46. Sayed, R.K.A., Fernández-Ortiz, M., Diaz-Casado, M.E., Rusanova, I., Rahim, I., Escames, G., López, L.C., Mokhtar, D.M., and Acuña-Castroviejo,

D. (2018). The Protective Effect of Melatonin Against Age-Associated, Sarcopenia-Dependent Tubular Aggregate Formation, Lactate Depletion, and Mitochondrial Changes. J. Gerontol. A Biol. Sci. Med. Sci. *73*, 1330–1338. https://doi.org/10.1093/gerona/gly059.

47. Barriocanal-Casado, E., Cueto-Ureña, C., Benabdellah, K., Gutiérrez-Guerrero, A., Cobo, M., Hidalgo-Gutiérrez, A., Rodríguez-Sevilla, J.J., Martín, F., and López, L.C. (2016). Gene Therapy Corrects Mitochondrial Dysfunction in Hematopoietic Progenitor Cells and Fibroblasts from Coq9R239X Mice. PLoS One *11*, e0158344. https://doi.org/10.1371/journal.pone.0158344.

48. Mohun, T.J., and Weninger, W.J. (2012). Embedding embryos for high-resolution episcopic microscopy (HREM). Cold Spring Harb. Protoc. *2012*, 678–680. https://doi.org/10.1101/pdb.prot069583.

49. Wendling, O., Hentsch, D., Jacobs, H., Lemercier, N., Taubert, S., Pertuy, F., Vonesch, J.L., Sorg, T., Di Michele, M., Le Cam, L., et al. (2021). High Resolution Episcopic Microscopy for Qualitative and Quantitative Data in Phenotyping Altered Embryos and Adult Mice Using the New "Histo3D" System. Biomedicines *9*, 767. https://doi.org/10.3390/biomedicines9070767.

50. Martínez-Martínez, M.A., Pacheco-Torres, J., Borrell, V., and Canals, S. (2014). Phenotyping the central nervous system of the embryonic mouse by magnetic resonance microscopy. Neuroimage *97*, 95–106. https://doi.org/10.1016/j.neuroimage.2014.04.043.

51. Diaz, F., Garcia, S., Padgett, K.R., and Moraes, C.T. (2012). A defect in the mitochondrial complex III, but not complex IV, triggers early ROS-dependent damage in defined brain regions. Hum. Mol. Genet. *21*, 5066–5077. https://doi.org/10.1093/hmg/dds350.

STAR★METHODS

KEY RESOURCES TABLE

REAGENT or RESOURCE	SOURCE	IDENTIFIER
Antibodies		
COQ2	Origene/Quimigen	Cat# TA341982; RRID: AB_3096491
COQ5	Novus Biologicals	Cat# NBP2-82738; RRID: AB_3096493
COQ4	Proteintech	Cat# 16654-1-AP; RRID: AB_2878296
COQ7	Proteintech	Cat# 15083-1-AP; RRID: AB_2082207
VDAC	Abcam	Cat# ab14734; RRID: AB_443084
GFAP	Millipore	Cat# MAB360; RRID: AB_11212597
NeuN	Abcam	Cat# ab104224; RRID: AB_10711040
MBP	Abcam	Cat# ab218011; RRID: AB_2895537
IBA-1	FUJIFILM Wako	Cat# 019-19741; RRID: AB_839504
Goat anti-Rabbit IgG (H + L) Secondary Antibody, HRP	Thermo Fisher	Cat# 31460; RRID: AB_228341
HRP Goat anti-mouse Ig	BD Pharmigen	Cat# 554002; RRID: AB_395198
Anti-mouse Alexa 594	Abcam	Cat# ab150116; RRID: AB_2650601
Anti-Rabbit Alexa 488 conjugated	Abcam	Cat# ab150077; RRID: AB_2630356
Chemicals, peptides, and recombinant proteins		
Bouin's Fluids	Thermo Fisher	Cat# 7211
Paraformaldehyde	Panreac Applichem	Cat# 2.529.311.315
Ethanol Absolute	VWR	Cat# 20821.330
Mayer's Hematoxylin solution	Sigma-Aldrich	Cat# MHS16
Eosin Y Solution	Sigma-Aldrich	Cat# HT110116
Periodic Acid	Sigma-Aldrich	Cat# P7875-25G
Schiff Reagent	Sigma-Aldrich	Cat# 3952016
Xylene (isomeric mixture)	Sigma-Aldrich	Cat# 1.08298.4000
Permount Mounting Media	Thermo Fisher	Cat# 15832544
ProLong™ Gold Antifade Mountant with DAPI	Thermo Scientific	Cat# P36931
Ammonium Chloride	Sigma-Aldrich	Cat# A4514
Sodium Citrate	Panreac Applichem	Cat# 1.416.551.211
4-Hydroxybenzoic acid	Sigma-Aldrich	Cat# H20059
Gadovist	Bayer	Cat# 735506.9
Top Vision Agarose	Thermo Scientific	Cat# R0491
Coenzyme Q_9	Sigma-Aldrich	Cat# 27597
Coenzyme Q_{10}	Sigma-Aldrich	#Cat C9538
Glacial Acetic Acid HPLC	VWR (Panreac)	Cat# 3.610.081.612
Sodium Acetate	Sigma-Aldrich	Cat# 3691771
2-Propanol HPLC	Sigma-Aldrich	Cat# 34863
1-Propanol HPLC	Sigma-Aldrich	Cat# 34871
Ethanol HPLC	Scharlau	Cat# ME03062500
Methanol HPLC	Scharlau	Cat# ME03062500
SDS	Sigma-Aldrich	Cat# L3771
Hexane	Sigma-Aldrich	Cat# 650552
DNAse/RNAse free water	VWR	Cat# E476
Agarose	Thermo Fisher	Cat# BP164-500
RedSafe	Sical (Intron)	Cat# 21141
PMSG	MSD Animal Health	Cat# 581135.2

(*Continued on next page*)

Continued

REAGENT or RESOURCE	SOURCE	IDENTIFIER
HCG	DFV Divasa Farmavic	Cat# 573676.1
TRI Reagent Solution (Trizol)	Thermo Fisher	Cat# AM9738
Cloroform	VWR	Cat# 83626-320
Loading Dye	Thermo Fisher	Cat# R0611
RIPA Buffer	Thermo Scientific	Cat# 89900
Halt Protease and Phosphatase Inhibitor Cocktail	Thermo Scientific	Cat# 78440
EDTA	Sigma-Aldrich	Cat# ED4SS
2-Mercaptoethanol	BIO-RAD	Cat# 161-0710
Laemli Sample Buffer	BIO-RAD	Cat# 161-0747
TGS	BIO-RAD	Cat# 161-0772
Spectra Multicolor Broad Range Protein Ladder	Thermo Scientific	Cat# 26634
Phosphate Buffered Saline	Fisher Bioreagents	Cat# BP399-20
Tween 20 Ultrapure	Thermo Scientific™	Cat# J20605.AP
Clarity Western ECL Substrate	Biorad	Cat# 1705061
Stripping Buffer	LabClinics	Cat# 60-0088
Fatty acid-free Bovine Serum Albumin	Sigma-Aldrich	Cat# A7030
Bradford Reagent	VWR	Cat# M172
TRIS	Panreac Applichem	Cat# 131940.1211
Succinate	Sigma-Aldrich	Cat# S2378
Sodium Piruvate	Fisher Scientific	Cat# 11360-070
Rotenone	Sigma-Aldrich	Cat# R8875
Oligomycin from Streptomyces diastatochromogenes	Sigma-Aldrich	Cat# O4876
Acetil coenzimaA trisodium salt	Sigma-Aldrich	Cat# A2056
Adenosine 5′-diphosphate sodium salt	Sigma-Aldrich	Cat# A2754
5,5′-Dithiobis(2-nitrobenzoic acid)	Sigma-Aldrich	Cat# D-8130
Carbonyl cyanide 4-(trifluoromethoxy)phenylhydrazone	Sigma-Aldrich	Cat# C292
Cytocrome C	Sigma-Aldrich	Cat# C7752
D-Manitol	Thermo Fisher	Cat# 125340010
EGTA	Sigma-Aldrich	Cat# E4378
HEPES	Sigma-Aldrich	Cat# H4034
L-Glutamic acid monosodium salt hydrate	Sigma-Aldrich	Cat# G1626
Magnesium chloride	Sigma-Aldrich	Cat# 5927
NADH	Sigma-Aldrich	Cat#N6005
Oxaloacetic acid	Sigma-Aldrich	Cat# O4126
Potasium Phosphate	Sigma-Aldrich	Cat# P3786
Potassium cyanide	Sigma-Aldrich	Cat# 60178
Potassium phosphate, monobasic	Thermo Fisher	Cat# 212595000
Sacarose	Sigma-Aldrich	Cat# S-0389
Hydrochloric Acid	Scharlau	Cat# AC07361000
DMEM (1X) + GlutaMAX	Gibco	Cat# 61965-059
FBS	Thermo Fisher	Cat# 11573397
Amino acids	Thermo Fisher	Cat# 11350912
Normocin	Ibian	Cat# ant-nr-2
DMSO	Thermo Fisher	Cat# 67-68-5
L-Glutamine 200mM (100X)	Gibco	Cat# 11500626
Glucose	Panreac Applichem	Cat# 1.413.411.210

(*Continued on next page*)

Continued

REAGENT or RESOURCE	SOURCE	IDENTIFIER
CARBONYL CYANIDE (trifluoromethoxy)phenyl hidrazone (FCCP)	Sigma-Aldrich	Cat# C2920-10MG
Antimycin A	Sigma-Aldrich	Cat# A8674
Perchloric acid	Panreac Applichem	Cat# 142175
KOH	Sigma-Aldrich	Cat# 1.050.331.000
Tetrabutylammonium hydrogen sulfate	Sigma-Aldrich	Cat# T-7158
DMEM (1X) -Glucose	Gibco	Cat# 11966-025
Potassium Dihydrogen Phosphate	Acros	Cat# 212595000
XF Assay Medium Modified DMEM	Agilent Technologies	Cat# 102365-100
Trypan Blue	Gibco	Cat# 15250-061
Critical commercial assays		
Mouse Direct PCR Kit	Deltaclon	CAT #B40015
MINI-PROTEAN TGX Gels 4–20% 10-well, 30	BIO-RAD	Cat# 456-1093
Trans-Blot Turbo Transfer Pack	BIO-RAD	Cat# 1704156
Brilliant III Ultra-Fast qPCR Master Mix	Agilent	Cat# 600880
High capacity cDNA reverse transcription kit	Thermo Fisher	Cat# 4368814
Seahorse XFe24 FluxPak	Agilent	Cat# 102340-100
Experimental models: Cell lines		
See Table S1		N/A
Experimental models: Organisms/strains		
Mouse: *Coq2*^{A252V}	This paper	N/A
Oligonucleotides		
Primer: 3' - GGACCAGGTTAAAATGCAGGC - 5′	Applied Biosystems	N/A
Primer: 3' - AGGGGACCTTGGGGAAGTTA - 5′	Applied Biosystems	N/A
Taqman probe (FAM) Coq2 Hs00794260_m1	Applied Biosystems	Cat# 4331182
Taqman probe (FAM) Coq4 Hs01082542_m1	Applied Biosystems	Cat# 4331182
Taqman probe (FAM) Coq5 Hs00260456_m1	Applied Biosystems	Cat# 4331182
Taqman probe (FAM) Coq7 Hs01029186_m1	Applied Biosystems	Cat# 4331182
Taqman probe (VIC) Gapdh Hs99999905_m1	Applied Biosystems	Cat# 4448484

RESOURCES AVAILABILITY

Lead contact

Further information and requests for resources and reagents should be directed to and will be fulfilled by the lead contact, Luis C. López (luisca@ugr.es).

Materials availability

This study did not generate new unique reagents. Samples from *Coq2*^{A252V} can be requested in collaborative bases.

Data and code availability

- All data reported in this paper will be shared by the lead contact upon request.
- This paper does not report original code.
- Any additional information required to reanalyze the data reported in this paper is available from the lead contact upon request.

EXPERIMENTAL MODEL AND STUDY PARTICIPANT DETAILS

Human skin fibroblasts

Control and mutant skin fibroblasts were obtained from patients with four different pathogenic variants in the *COQ2* gene (Table S1), after the writing informed consent was obtained in the respective medical institutions.

Generation of the Coq2^{A252V} mouse model

A 8.8 kb region used to construct the targeting vector was subcloned from a positively identified C57BL/6 BAC clone (RP23-298K24) using homologous recombination-based techniques. The vector was designed such that the A252V (GCC > GTC) point mutation is introduced in exon 5 of the *Coq2* gene. A Neomycin selection marker with flanking FRT sites is positioned downstream of exon 5. The 5′ long homology arm (LA) of the vector is ~6 kb in length and the 3′ short homology arm (SA) is ~2.5 kb (Figure S8A). The targeting vector was confirmed by restriction analysis and sequencing after each modification step. The boundaries of the vector and genomic sequences were confirmed by sequencing primers SEQ5′ and SEQ3′ which read from inside the backbone. The point mutation was confirmed by sequencing using primer ivNeoN3. The FRT sequences on the *Neo* cassette were confirmed by iNeoN2 and IVNeoN3, which read from inside the *Neo* selection marker.

The targeting vector (10 μg) was linearized and then transfected by electroporation of FLP C57BL/6 (BF1) embryonic stem cells. After selection with G418 antibiotic, surviving clones were expanded for PCR analysis to identify recombinant ES clones (Figures S8B–S8E). The *Neo* cassette in targeting vector has been removed during ES clone expansion (inGenious Targeting Laboratory, NY, USA) (Figures S8B–S8E). Targeted iTL BF1 (C57BL/6 FLP) embryonic stem cells were microinjected into Balb/c blastocysts. Resulting chimeras with a high percentage black coat color were mated to C57BL/6N WT mice to generate Germline *Neo* Deleted mice (Figure S8F) (inGenious Targeting Laboratory, NY, USA). Tail DNA was analyzed as described below from pups with black coat color. Heterozygous mice for the knockin allele were crossbreed to obtain wild-type controls (*Coq2*$^{+/+}$), heterozygous knockin (*Coq2*$^{+/A252V}$) or homozygous knockin (*Coq2*$^{A252V/A252V}$ = *Coq2*^{A252V}) mice. The animals were housed in the Animal Facility of the University of Granada under an SPF zone on a 12-h light/dark cycle with unlimited access to water and food. All animal manipulations and experiments were performed according to a protocol approved by the Institutional Animal Care and Use Committee of the University of Granada (procedure number 30/06/2022/097) and were in accordance with the European Convention for the Protection of Vertebrate Animals used for Experimental and Other Scientific Purposes (CETS#123), the Spanish law (R.D. 53/2013) and the ARRIVE guidelines. In the analytical experiments, we used an equal number of male and female mice. Animals were utilized at embryonic stages (E15.5 or E17.5) or at the age of one month, unless otherwise specified.

METHOD DETAILS

Cell culture and treatment

Fibroblasts were cultured at 37°C and 5% CO_2 in high glucose DMEM-GlutaMAX medium supplemented with 10% FBS, 1% MEM non-essential amino acids, and 1% antibiotics/antimycotic. Fibroblasts were treated with 1 mM 4-hydroxybenzoic acid during 7 days. 4-hydroxybenzoic acid was dissolved in 4% DMSO, giving a final concentration of DMSO in cell culture of 0.04%. After treatment, cells were collected and analyzed. A control group with vehicle at the same dose was studied. To assess cell viability and the measurements of adenosine nucleotides, cells were cultured in galactose media, which forces energy production through oxidative phosphorylation.[43–45] Galactose medium consisted in free-glucose DMEM-GlutaMAX medium supplemented with 10% dialyzed FBS, 1% MEM non-essential amino acids, and 1% antibiotics/antimycotic.

Treatment in mice

4-hydroxybenzoic acid (4HB) (Merck Life Science S.L.U, Madrid, Spain) was given to the mice in the chow at a concentration of 0.33% (w/w). Pregnant mice began receiving the assigned treatment, and the offspring continue receiving the treatment after weaning (Figure S7). Therefore, animals receive the treatment through the placenta (embryonic development), the breast milk (after birth) and the chow (after weaning). Animals were randomly assigned to experimental groups. Data were randomly collected and processed.

Mouse phenotyping

Body weight was recorded once a week. To assess motor and sensorimotor performance the following test were performed in animals at one month of age: 1) negative geotaxia, consisting in measuring the time taken to turn 180° after being placed upside down on a ramp inclined at 45°; 2) beam test, consisting in measuring the time to cross a 1 m long bar with a 1 cm wide surface held at a height of 50 cm; 3) pole test, consisting in the evaluation of the ability of a mouse to grasp on a pole to descend to its home cage. Mice are placed head oriented upward on top of the pole; 4) rotarod, consisting in measuring the latency to fall from an accelerating rotarod beginning at 0 rpm and accelerating to 40 rpm at 0.13 rpm/s for 240 s. Mice were trained one day before the initial test.[38,39] All tests were analyzed by two different examiners blinded to the experimental group.

Running distance and time of exhaustion were tested by using a treadmill system (Panlab LE 8710 Treadmill control, Barcelona, Spain).[46] Because behavioral variability between individuals of the same group is high, the environmental variables must be constant throughout the study (light, humidity, background, and noise) as well as time, age, and the sex of the animal. Before experiments with treadmill, the animals were prior adapted for 3–5 days at a constant rate of 9 cm/s for 20 min to become familiar with the apparatus. At the day of experiment, the body weight of the animals was measured, and the apparatus speed was initially adjusted at 9 cm/s for 5 min and then the speed was increased 2 cm/s every minute until the mouse reached exhaustion. The point of exhaustion was considered when the mouse received 50 electric stimuli.

Quantification of CoQ_9 and CoQ_{10} levels

Tissue lipid extraction was performed by mixing tissue homogenate with 1-propanol. After vortexing 30 s, the mix was centrifuged at 11,300 g for 5 min. The resulting supernatant was injected into the HPLC system using a reverse-phase C18 3.5 mm, 4.6 × 150 mm column (Waters, Spain) and a mobile phase consisting of methanol, ethanol, 2-propanol, acetic acid (500:500:15:15) and 50 mM sodium acetate at a flow rate of 0.9 mL/min.[24] Cells lipid extraction was performed by mixing cells homogenate with 50 mM SDS and a proportion 2:1 of hexane:ethanol. After vortexing 2 min in a glass tube, the mix was centrifuged at 2,000 g for 5 min (twice). The upper phase is transferred to a glass tube and evaporated with nitrogen gas. The residue was resuspended in 1-propanol.[44] CoQ_9 and CoQ_{10} levels were determined in the resultant extract via reversed-phase HPLC coupled to electrochemical detection, as previously described.[24] Then, a standard curve of CoQ_9 was used for a quantitative estimation. Results were normalized by milligram proteins, which were quantified in tissue or cell homogenates using Bradford assay. The results were expressed in nanograms of CoQ per milligram of protein.

Assessment of mitochondrial respiration

Oxygen consumption rate (OCR) was measured in adherent skin fibroblasts with a XF[24] Extracellular Flux Analyzer (Seahorse Bioscience, Billerica, MA, USA). Each cell line was seeded in 6 wells of a XF[24]-well cell culture microplate (Seahorse Bioscience) at a density of 5×10^4 cells/well in 250 μL of DMEM and incubated for 24 h at 37°C in 5% CO_2 atmosphere. After replacing the growth medium with 525 μL of bicarbonate-free DMEM pre-warmed at 37°C cells were preincubated for 1 h in a CO_2 free incubator before starting the assay procedure.[47] After baseline measurements, OCR was measured after sequentially adding to each well 75 μL of oligomycin, 75 μL of carbonyl cyanide 4-(trifluoromethoxy) phenylhy-drazone (FCCP) and 75 μL of rotenone and antimycin, to reach working concentrations of 1 μM, 0.75 μM, and 1 μM, respectively.[47] Spare respiratory capacity was calculated according to the User Manual XF cell Mito-Stress test kit (SeaHorse Biosciences). Spare respiratory capacity = (Maximal respiration) - (Basal Respiration). Non-mitochondrial respiration was subtracted in both maximal respiration and basal respiration. Spare respiratory capacity provides an idea of the cells maximum ATP production; therefore, cells with a higher capacity have a greater ability to respond to stress.

Mitochondrial isolation from the kidneys and liver was performed as previously described.[39] Mitochondrial respiration was measured using an XF^{e}[24] Extracellular Flux Analyzer (Seahorse Bioscience).[39] Mitochondria were first diluted in cold MAS 1X for plating (1.5 μg/well). Next, 50 μL of mitochondrial suspension was delivered to each well (except for background correction wells) while the plate was on ice. The plate was then centrifuged at 2,000g for 10 min at 4°C. After centrifugation, 450 μL of MAS 1X + substrate (10 mM succinate, 2 mM malate, 2 mM glutamate and 10 mM pyruvate) was added to each well. Respiration by the mitochondria was sequentially measured in a coupled state with the substrate present (basal respiration or State 2) followed by State 3° (phosphorylating respiration, in the presence of ADP and substrates). State 4 (non-phosphorylating or resting respiration) was measured after addition of oligomycin when all ADP was consumed, and then maximal uncoupler-stimulated respiration was measured by FCCP (State 3u). Injections were as follows: port A, 50 μL of 40 mM ADP (4 mM final); port B, 55 μL of 30 μg/mL oligomycin (3 μg/mL final); port C, 60 μL of 40 μM FCCP (4 μM final); and port D, 65 μL of 40 μM antimycin A (4 μM final). All data were expressed in pmol/min/mg protein.

Assessment of CoQ-dependent respiratory chain activities

CoQ-dependent respiratory chain activities were measured in tissue samples of brain. Tissue samples were homogenized in CPT medium (0.05 M Tris-HCl, 0.15 M KCl, pH 7.5) at 1100 rpm in a glass–Teflon homogenizer. Homogenates were sonicated and centrifuged at 600 g for 20 min at 4°C, and the supernatants obtained were used to measure CoQ-dependent respiratory chain activities (CI + III and CII + III) as previously described.[16] The results were expressed in nmol reduced cyt *c*/min/mg prot and nmol reduced cyt *c*/min/citrate synthase activity. The citrate synthase activity was measured, with the previously obtained supernatants, at 30°C in the presence of 0.3 mM acetyl-CoA and 0.1 mM DTNB (5,5-dithio-bis-(2-nitrobenzoic acid)). The reaction was initiated by the addition of 0.5 mM oxalacetate and the absorbance was monitored at 412 nm.

Measurement of adenosine nucleotides levels

Fibroblasts cultured under glucose-free media supplemented with galactose possess ATP and ADP pools that are predominantly dependent on the oxidative phosphorylation[43]; therefore, using these culture conditions, ATP levels and ATP/ADP ratio are reliable markers of oxidative phosphorylation and correlate with the rates of ATP synthesis in CoQ_{10} deficient cells, as reported.[44,45] To determine the adenine nucleotides levels, cells were grown in 15-cm-diameter plates to 90% confluency and the adherent cells were collected in ice-cold PBS using a scraper. After centrifugation at 3,000 *g* for 3 min at 4°C, pellets were suspended in 200 μL of ice-cold 0.5 M perchloric acid, vortexed for 30 s, and centrifuged at 11,000 *g* for 10 min at 4°C. Pellets were stored at −80°C for protein measurement. Adenine nucleotides were measured in the supernatants injected into an Alliance HPLC (Waters Corporation, Milford, MA, USA) with an Alltima C18 NUC reverse-phase column (Alltech Associates, Deerfield, IL, USA).[44,45] Adenine nucleotide levels were expressed in nmol/mg protein. ATP/ADP ratio was calculated as an indirect assessment of the OxPhos function.

Assessment of cell death

Measurement of cell viability was performed with the Trypan blue exclusion method. Numbers of living and dead adherent cells were determined by the Countess automated cell counter (Invitrogen).[44] All cells were counted and results were expressed as percentage of dead cells relative to total cells.

Histology and immunohistochemistry

Tissues were fixed in formalin (24 h), processed and embedded in paraffin. Multiple sections (4 μm thickness) were deparaffinized with xylene and stained with hematoxylin and eosin (H&E) or Periodic Acid-Schiff Stain (PAS) (Merck Life Science S.L.U, Madrid, Spain).

To identify neurons (NeuN, 1:300, Merck Milipore), myelin (anti-MBP, 1:500 Abcam), astrocytes (GFAP, 1:500 Sigma Aldrich) and microglial activation (Iba1, 1:500, Wako), immunohistochemistry was performed. Briefly, after deparaffination, sections were boiled using 0.1 M sodium citrate buffer at pH 6, heating at 90C in a water bath for 40 min. After numerous washes in phosphate-buffered saline (PBS, 0.1 M, 0.02% Triton X-100), sections were incubated with the primary antibody at 4°C overnight. Then, secondary antibodies conjugated with Alexa Fluor 488 or 594 were used at 37°C during 2h. Finally, the slides were mounted with ProLongTM Gold Andifade Mountant with DAPI (Invitrogen).

Sections were examined at 40–400 magnifications with a Nikon Eclipse Ni-U microscope (Werfen, Madrid, Spain), and the images were scanned under equal light conditions with the NIS-Elements Br computer software (Werfen, Madrid, Spain).

High-resolution episcopic microscopy (HREM)

E15.5 embryos were fixed in Bouin's fixative for 24 h, then washed and stored in 70% EtOH. Fixed samples were gradually dehydrated in an increasing series of ethanol concentrations and were embedded in a methacrylate resin (JB-4 kit, Polysciences, Warrington, PA) containing eosin and acridin orange as contrasts agents as previously described.[48] The resin blocks were sectioned on the Histo3D system to generate data by repeated removal of 7 μm thick sections.[49] Resulting HREM data with a voxel size of 8 × 8 × 7 μm3 (E15.5 whole embryos) were generated from approximately 800 aligned images. All HREM images were converted into a volume dataset and segmented using Avizo 9.4.0 software (Thermofisher Scientific, France) to create 2- and 3-dimensional (3D) images, according to the Allen brain atlas.

In vivo MRI and proton MRS

In embryos, MRI experiments were carried out on a 9.4 T Bruker Biospec MRI system (Bruker BioSpin, Ettlingen, Germany) equipped with 400 mT m-1 field gradients and a 40 mm quadrature bird-cage resonator. Godavist, administered intraperitoneally (12.5 mL/g b.w.) in female mice at 17.5 days of pregnancy, was used as contrast agent.[50] E17.5 embryos were fixed in 4% PFA overnight at 4°C, and embedded in 4% low melting agarose. Falcon tubes containing the embryos embedded in agarose were placed in a mouse cradle and positioned at the isocenter of the magnet.[50] High-resolution 3D images of whole embryos were acquired using a 3D Turbo RARE sequence with the following parameters: TEeff = 45 ms, TR = 1000 ms, RARE factor = 16, FOV = 22 × 11 × 14.66 mm3, matrix size = 384 × 192 × 256, resulting in an isotropic resolution of 57 μm, 20 averages (total acquisition time of approximately 24 h), and 6 out-of-volume saturation bands in all three acquisition directions.

In adults' animals, magnetic resonance imaging and MRS studies were conducted using a 7 T horizontal bore magnet Bruker Biospec TM 70/20 USR designed for small animal experimentation. Following localizer scans, high-resolution axial and coronal T2-weighted datasets were acquired in order to visualize any cerebral or structural atrophy and to investigate for potential focal pathologies.[38,51]

QUANTIFICATION AND STATISTICAL ANALYSIS

No statistical method was used to determine sample size. Statistical analyses were performed using the Prism 9 scientific software. In the figures, each point represents a biological replicate and data are expressed as the mean ± SD. A one-way or two-way ANOVA was used to compare the differences between experimental groups. Post hoc correction for multiple comparisons was made using Tukey's or Sidak's tests when appropriate. A p-value of <0.05 was considered to be statistically significant. Survival curve was analyzed by log rank (Mantel-Cox) and the Gehan–Breslow–Wilcoxon tests. All the statistical parameters can be found in the figures and figure legends.